Int. J. Multiphase Flow Vol. 14, No. 4, pp. 425–438, 1988
Printed in Great Britain.

0301-9322/88 $3.00 + 0.00

PHASE DISTRIBUTION DURING STEAM–WATER FLOW IN A HORIZONTAL T-JUNCTION

M. T. RUBEL,† H. M. SOLIMAN and G. E. SIMS
Department of Mechanical Engineering, University of Manitoba, Winnipeg, Manitoba R3T 2N2, Canada

(*Received* 2 *June* 1987; *in revised form* 22 *January* 1988)

Abstract—Data are presented for the phase distribution of low-pressure steam–water mixtures at a dividing T-junction (in which the inlet flow is split into two streams, one continuing in the same direction while the other is diverted at a right angle to the inlet direction). All three sides of the junction have the same diameter (37.6 mm i.d.) and all are in the same horizontal plane. The data cover ranges of inlet mass flux and inlet quality which produced a number of flow patterns, as well as a wide range of extraction rates. The influence of relevant independent parameters on phase distribution was investigated and comparisons with existing empirical and analytical correlations resulted in good agreement.

Key Words: two-phase flow, horizontal, dividing T-junction, steam–water

1. INTRODUCTION

Phase distribution in branching conduits has been receiving considerable attention lately due to its direct application to many flow situations encountered in the power and process industries. Given a branching junction with known geometry and orientation, it is necessary to develop predictive models for evaluating the fractions of one phase leaving through each outlet port for given outlet fractions of the second phase and inlet flow conditions. Operation, maintenance and efficiency of many engineering components depend on the manner in which the phases are distributed at branching junctions.

Several investigations have been carried out, most of which have appeared in the literature during the past 10 years, and each of which has contributed to our present understanding of the problem. These investigations showed clearly that the two phases are generally not distributed evenly among outlet ports, but the manner in which the phases are distributed is not yet fully-established. The most recent experimental investigations include those of Collier (1975), Hong (1978), Henry (1981), Azzopardi & Whalley (1982), Azzopardi (1984), Saba & Lahey (1984) and Seeger *et al.* (1986). These investigations demonstrated that the ratio of branch to inlet qualities x_3/x_1, which is indicative of phase distribution, is influenced by several parameters such as the inlet flow pattern, inlet quality x_1, branch-to-inlet diameter ratio D_3/D_1, branch orientation (from vertically up to vertically down) and extraction rate W_3/W_1, where W_1 and W_3 are the inlet and branch mass flow rates, respectively. An extensive review of literature on this topic was published recently by Azzopardi (1986).

A few predictive models have been proposed. These include the analytical model by Saba & Lahey (1984) which was found to be applicable only to dispersed bubble flow with high extraction rates (Lahey 1986), a phenomenological model by Azzopardi & Whalley (1982) for annular flow, an empirical model by Seeger *et al.* (1986) and a recently proposed analytical model by Hwang *et al.* (1988). Further extensive testing is required to establish one or a combination of these models as the recommended predictive tool.

The purpose of this investigation is to develop new phase-distribution data under operating conditions not yet reported in the open literature. In addition to enhancing the current understanding of the phenomenon, this new data can provide an important test of the available models. The geometry under consideration is that of a 90° T-junction where all three pipes (inlet, run and branch) are of the same diameter (37.6 mm i.d.), all in the horizontal plane and the flow enters along the straight-through direction. The range of conditions to be tested in the present experiment is that of low inlet mass flux ($15 < G_1 < 50\,\text{kg/m}^2\,\text{s}$) and low pressure

†Current address: Texaco Canada Resources, Edmonton, Alberta T5K 2K4, Canada.

($100 < P < 250$ kPa) steam–water mixtures with wide ranges of inlet qualities ($20 < x_1 < 90\%$) and extraction rates ($0.15 < W_3/W_1 < 0.8$).

2. EXPERIMENTAL INVESTIGATION

The experimental facility used in this investigation is shown schematically in figure 1. The flow loop used to provide stream–water mixtures to the horizontal, T-junction test section is capable of the following operating conditions: total mass flow rates (steam + water) up to 200 kg/h, mixture pressures ranging between 100 and 250 kPa, qualities at test section inlet (x_1) ranging between 20 and 80% and branch extraction rates (W_3/W_1) from 0.2 to 0.8. A brief description of the flow circuit is provided below and further details were reported by Rubel (1986).

2.1. Flow loop

A controllable amount of steam was generated in the boiler from distilled water. Building steam, at a regulated pressure of 850 kPa, was used as the heat source in the boiler. The generated steam was first passed through a superheater which allowed control of the degree of superheat at its exit. After measuring the pressure and temperature, the superheated steam was passed through a precondenser where cooling water was used to partially condense the steam to any desired quality. The pressure and temperature were again measured at the exit of the precondenser. The two-phase mixture was then allowed to develop in a straight adiabatic length for 37 tube dia after which the inlet flow pattern was observed through a specially designed visual section. A further 56 tube dia of straight adiabatic developing length was provided before the flow reached the T-junction. The test section is shown schematically in figure 2.

In order to ensure consistency with other research laboratories, a square-edged T-junction was designed and constructed. This required precision machining, thereby eliminating any rounded edges or interior burrs and ensuring close tolerances. The T-junction, as shown in figure 3, consisted of two main components: a main body and a branch section. The main body was machined from a 63.5 mm square brass bar, 126 mm long. This length was chosen to allow the inlet and run copper tubing to mate with the T-junction for 38 mm, thus maintaining the coaxiality of the assembly. The branch section was machined from a 76 mm dia brass rod, 44.5 mm long.

Throttling valves, located far downstream in both the branch and run sides, controlled the fractions of the two-phase mixture entering each side. After the flow patterns in both the branch and run had been observed through visual sections, each of the two-phase mixtures entered its respective separation tank. In these tanks the steam and water were separated, while maintaining a steady liquid level in each tank. The steam from each tank was passed through an aftercondenser and the resulting condensate flow was measured by the appropriate (one or any combination of a possible four) flowmeters, arranged in parallel. This provided individual measurements of W_{G2}

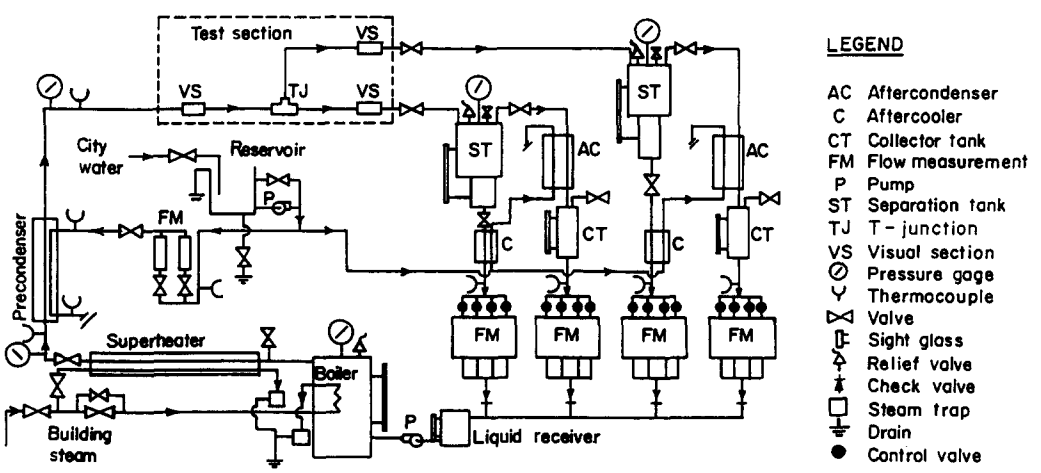

Figure 1. Schematic diagram of experimental facility.

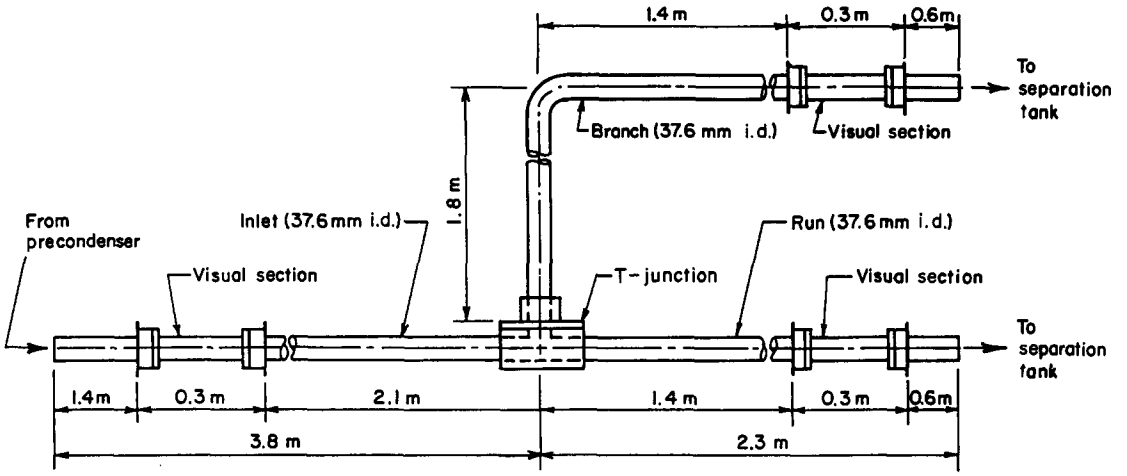

Figure 2. Schematic diagram of the test section.

and W_{G3}, the vapor-phase flow rates in the run and branch, respectively. The liquid phase from each separation tank passed through an aftercooler and the flow rate was also measured by one or more of four flowmeters in parallel, thus providing measured values for W_{L2} (run) and W_{L3} (branch). The two lines of condensate and two lines of liquid were then rejoined and collected in a liquid receiver tank before returning back to the boiler to complete the cycle.

It was recognized that accurate measurements of W_{G2}, W_{G3}, W_{L2} and W_{L3} were crucial for this investigation and that these four quantities could vary over wide ranges depending on W_1, x_1 and W_3/W_1. This necessitated an elaborate flow-measuring station (shown in figure 1) and specially desgined separation tanks downstream from the branch and run sides. The tanks incorporated an abrupt change in cross-sectional area at about mid-height. If the flow rate into one particular tank was low, the vapor–liquid interface was maintained in the smaller-diameter section of the tank and vice versa.

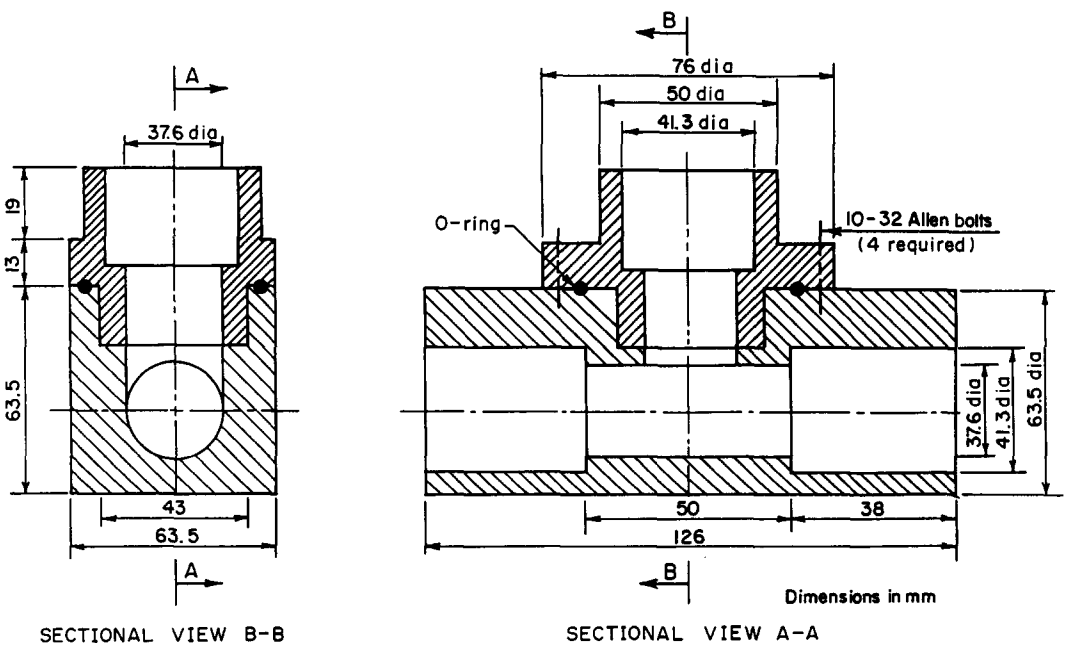

Figure 3. Cross-sectional views of the T-junction.

Before any testing began, all thermocouples, pressure gages and flowmeters were calibrated, the horizontality of the test section was checked by a surveying transit and the whole flow loop was tested against leakage. The flow loop, except for the visual sections, was covered by a 63 mm thick layer of fiberglass insulation to minimize heat losses.

2.2. Procedure

Phase-separation data were generated by performing a number of test groups covering the maximum possible range of W_1 and x_1 of which the experimental facility was capable. Each test group corresponded to approximately the same values of W_1 and x_1, and a number of test runs (each corresponding to a different extraction rate W_3/W_1) were carried out within each test group. It was noted that varying W_3/W_1 from one test run to the other within each group caused slight changes in W_1 and x_1 which were difficult to avoid.

During each test run, the following readings were monitored continuously: test-fluid pressure and temperature at different locations in the loop; liquid level in the separation, collector and receiver tanks; test-fluid flowmeters and cooling-water flowmeter; and inlet and exit temperatures in the precondenser. All these readings remained constant for at least 30 min before they were recorded. A typical test run required at least 2 h of continuous operation before steady-state conditions were reached; some runs with low W_1 required up to 4 h.

The individually measured values of vapor and liquid flow rates in both the branch and run sides were used to calculate W_1, x_1, W_3/W_1 and x_3 using the following simple relations:

$$W_{G1} = W_{G2} + W_{G3} \quad [1a]$$

$$W_{L1} = W_{L2} + W_{L3} \quad [1b]$$

$$W_1 = W_{G1} + W_{L1} \quad [1c]$$

$$x_1 = \frac{W_{G1}}{W_1} \quad [1d]$$

$$W_3 = W_{L3} + W_{G3} \quad [1e]$$

$$x_3 = \frac{W_{G3}}{W_3}, \quad [1f]$$

where W_{G1} and W_{L1} are the inlet vapor and liquid flow rates, respectively. Equations [1a] and [1b] assume no flashing, which is a reasonable assumption for the present test conditions of low mass flow rates and consequently low pressure drops across the junction sides. As a test on the accuracy of the present measurements, each experimental values of x_1 obtained from [1d] was compared with an independently calculated estimate of x_1. The independent estimate of x_1 was obtained from a simple heat balance on the precondenser using the measured values of pressure and temperature of the inlet superheated steam, the outlet pressure of the steam–water mixture, the mass flow rate of the mixture W_1 from [1c], the mass flow rate of the cooling water and inlet and outlet temperatures of the cooling water. Only runs where the deviation between the two values of x_1 came within $\pm$ 10% were accepted; actually, 64% of the recorded runs corresponded to deviations within $\pm$ 5%.

It is important to relate the phase-separation measurements to the observed flow patterns, particularly in the inlet side of the junction. In the present investigation, three major (stratified, wavy and semiannular) and one transitional (semiannular–wavy) flow patterns were visually observed. The following descriptions were used to identify the different flow patterns:

Stratified flow. The liquid flows along the bottom of the tube and the vapor on top of it with a smooth interface.

Wavy flow. The two phases are separated with liquid flowing at the bottom of the tube. The vapor–liquid interface is wavy, apparently due to a difference between the vapor and liquid velocities.

Semiannular–wavy flow. Similar to wavy flow in appearance, although the liquid begins to rise up the tube wall forming a film. The film is very thin and most of the liquid appears as a thick stratum at the bottom.

Semiannular flow. A stable liquid film covers the lower part of the tube wall and the upper portion of the tube appears dry. The liquid film thickness increases around the periphery with a maximum at the bottom of the tube. Some of the liquid phase may appear as droplets entrained in the vapor.

3. RESULTS AND DISCUSSION

Nineteen test groups containing 111 data points (or test runs) were generated in this investigation. The range of operating conditions covered by this data is:

inlet mass flux $G_1 = 16.1 - 50.3\ \text{kg/m}^2\,\text{s}$
inlet quality $x_1 = 21.4 - 86.8\%$
inlet pressure $P_1 = 111 - 232\ \text{kPa}$
inlet flow pattern = stratified, wavy, semiannular–wavy and semiannular
extraction rate G_3/G_1 (or W_3/W_1) = 0.15–0.80,

where G_3 is the mass flux in the branch. A detailed listing of all data points is given in table 1.

In order to show the range tested, the operating conditions corresponding to the present 19 test groups were plotted on the flow pattern map of Mandhane *et al.* (1974) using V_{LS} and V_{GS} as coordinates, where V_{LS} is the superficial liquid velocity given by $V_{LS} = (1 - x_1)G_1/\rho_L$, V_{GS} is the superficial vapor velocity given by $V_{GS} = x_1 G_1/\rho_G$, ρ_L is the liquid density and ρ_G is the vapor density. The result, shown in figure 4, indicates good agreement between the present visual observations of inlet flow patterns and the predictions of Mandhane *et al.* (1974).

Figure 5 shows a composite drawing illustrating the regions occupied by the data of different inlet flow patterns. The complexity of the problem is obvious with uneven phase distribution at the junction appearing to be the general rule. Preferential liquid flow into the branch occurred for all the present data of stratified flow while most of the wavy flow data showed preferential vapor flow into the branch. The semiannular flow data appear on both sides of the line of even phase distribution in figure 5.

In order to illustrate the trends in the present experiment, the data will be presented in a number of ways in an attempt to isolate the individual effects of important independent parameters. Comparisons with previous experimental trends will be included as they become relevant. Since $D_3 = D_1$ in the present study, the extraction rate will be denoted by G_3/G_1 or W_3/W_1, which are equal.

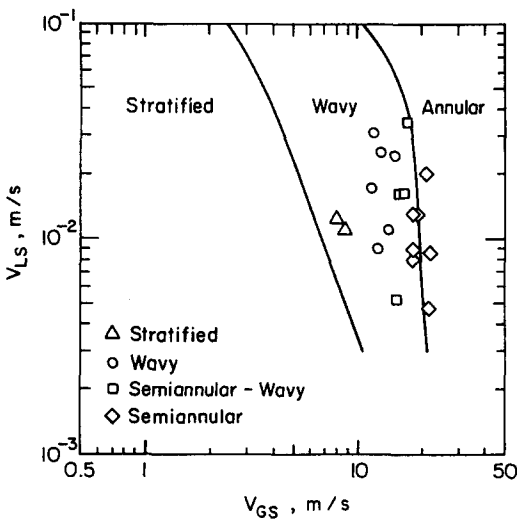

Figure 4. Operating conditions plotted on the flow pattern map of Mandhane *et al.* (1974).

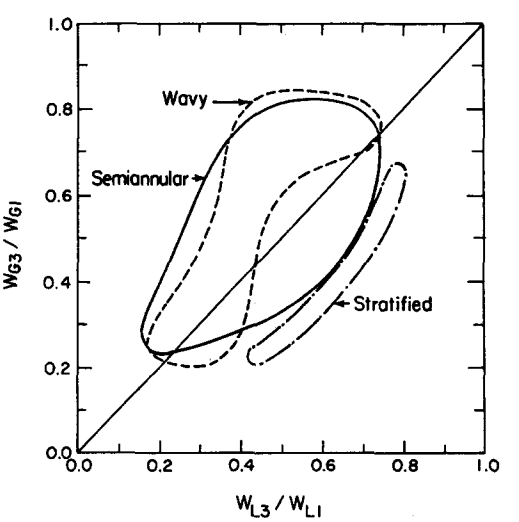

Figure 5. Phase-distribution data of different flow patterns.

Table 1. Operating conditions and phase-distribution data

No.	P_1 (kPa)	G_1 (kg/m^2 s)	x_1 (%)	$\frac{G_3}{G_1}$	$\frac{x_3}{x_1}$	Inlet flow pattern
1-1	136	29.6	38.7	0.265	1.36	
1-2	125	28.6	40.5	0.413	1.42	
1-3	150	32.1	41.6	0.512	1.38	Wavy
1-4	150	28.8	36.0	0.542	1.45	
1-5	142	28.5	35.7	0.624	1.33	
2-1	124	32.5	51.4	0.211	1.21	
2-2	167	32.5	54.4	0.378	1.16	
2-3	156	33.0	56.8	0.440	1.14	Semiannular–wavy
2-4	181	31.7	50.5	0.588	1.28	
2-5	205	30.7	51.2	0.682	1.24	
3-1	143	25.3	34.6	0.236	1.35	
3-2	129	24.9	35.7	0.476	1.35	
3-3	129	25.2	38.6	0.604	1.29	Wavy
3-4	139	24.5	34.2	0.722	1.10	
4-1	194	37.8	43.2	0.209	1.31	
4-2	156	39.8	43.5	0.402	1.24	
4-3	194	39.2	44.9	0.551	1.35	Wavy
4-4	208	38.9	39.8	0.575	1.41	
4-5	201	39.5	41.7	0.594	1.38	
4-6	208	39.4	40.5	0.622	1.36	
5-1	205	31.3	62.8	0.235	1.07	
5-2	211	31.2	62.5	0.257	1.08	
5-3	184	33.2	64.4	0.378	1.05	Semiannular
5-4	170	32.0	60.1	0.461	1.10	
5-5	170	32.9	65.9	0.481	1.04	
5-6	218	32.1	66.8	0.656	1.13	
5-7	215	31.7	61.5	0.668	1.17	
6-1	204	39.3	52.5	0.239	1.18	
6-2	198	39.3	51.7	0.296	1.18	
6-3	184	41.1	53.7	0.338	1.15	
6-4	187	41.4	53.7	0.344	1.17	Semiannular
6-5	170	43.0	55.8	0.435	1.16	
6-6	163	42.2	56.2	0.440	1.15	
6-7	187	39.0	53.6	0.548	1.25	
6-8	204	38.7	51.3	0.624	1.29	
7-1	222	33.6	71.7	0.302	0.980	
7-2	210	32.8	76.3	0.360	0.956	
7-3	197	33.7	76.3	0.412	0.972	Semiannular
7-4	177	34.3	78.5	0.507	0.984	
7-5	205	35.0	74.5	0.566	1.05	
7-6	232	32.4	75.4	0.687	1.08	
8-1	187	26.5	68.5	0.290	1.03	
8-2	184	27.8	68.6	0.350	1.04	
8-3	170	27.4	70.2	0.411	1.02	Semiannular
8-4	156	28.1	73.0	0.514	1.01	
8-5	201	26.9	66.2	0.702	1.12	
9-1	163	28.6	58.1	0.256	1.10	
9-2	156	29.4	59.1	0.320	1.11	Semiannular
9-3	135	29.1	61.4	0.465	1.08	
9-4	170	28.3	57.1	0.656	1.18	
10-1	191	25.8	81.0	0.305	0.943	
10-2	181	26.0	82.1	0.382	0.941	
10-3	173	26.4	84.4	0.421	0.937	Semiannular
10-4	156	28.0	86.8	0.527	0.949	
10-5	211	26.4	79.8	0.795	1.02	

continued

Table 1—*continued*

No.	P_1 (kPa)	G_1 (kg/m^2 s)	x_1 (%)	$\frac{G_3}{G_1}$	$\frac{x_3}{x_1}$	Inlet flow pattern
11-1	167	19.1	71.9	0.278	0.981	
11-2	158	19.5	72.4	0.340	1.01	
11-3	156	20.0	72.3	0.406	1.02	Semiannular–wavy
11-4	153	20.2	74.1	0.514	0.997	
11-5	153	18.9	74.1	0.570	1.01	
11-6	167	18.1	71.9	0.714	1.03	
12-1	181	24.3	66.2	0.225	1.04	
12-2	170	24.5	67.8	0.287	1.02	
12-3	163	25.3	69.3	0.355	1.02	Semiannular
12-4	156	25.7	71.2	0.394	1.01	
12-5	143	26.0	71.2	0.505	1.01	
12-6	184	25.4	65.7	0.715	1.09	
13-1	132	33.5	29.0	0.225	1.37	
13-2	129	33.7	31.7	0.280	1.45	Wavy
13-3	122	34.8	32.7	0.357	1.48	
13-4	153	34.1	27.8	0.689	1.20	
14-1	143	38.1	21.4	0.207	1.19	
14-2	136	38.1	23.0	0.233	1.38	
14-3	132	38.3	23.8	0.261	1.42	
14-4	129	38.8	24.5	0.267	1.47	Wavy
14-5	122	38.4	24.7	0.324	1.59	
14-6	132	39.3	23.9	0.445	1.61	
14-7	143	38.5	21.6	0.661	1.19	
15-1	184	49.1	30.8	0.153	1.38	
15-2	170	49.6	30.4	0.186	1.47	
15-3	163	49.0	32.9	0.230	1.49	Semiannular–wavy
15-4	149	48.3	33.5	0.277	1.51	
15-5	143	50.3	34.3	0.351	1.45	
15-6	150	48.5	33.5	0.399	1.56	
15-7	156	47.7	32.0	0.445	1.60	
16-1	132	17.1	48.0	0.308	0.774	
16-2	129	16.8	50.3	0.361	0.877	
16-3	127	17.1	51.3	0.397	0.922	
16-4	122	17.3	51.9	0.415	1.02	Wavy
16-5	115	17.8	54.3	0.474	1.06	
16-6	129	17.9	51.5	0.596	1.09	
16-7	129	16.8	51.2	0.728	0.987	
17-1	122	16.5	30.0	0.364	0.618	
17-2	115	16.1	31.8	0.466	0.694	
17-3	115	16.5	32.1	0.507	0.720	Stratified
17-4	115	16.8	32.2	0.532	0.739	
17-5	111	16.9	34.0	0.623	0.779	
17-6	116	16.5	32.6	0.733	0.917	
18-1	143	16.8	37.9	0.363	0.600	
18-2	136	16.6	39.7	0.484	0.688	
18-3	136	17.2	40.6	0.534	0.742	Stratified
18-4	129	16.9	42.7	0.557	0.744	
18-5	122	16.5	43.4	0.636	0.808	
18-6	136	16.8	41.2	0.741	0.879	
19-1	177	27.5	49.2	0.166	1.24	
19-2	170	28.6	52.0	0.245	1.19	
19-3	160	28.9	52.0	0.298	1.21	Semiannular–wavy
19-4	156	29.3	53.2	0.340	1.20	
19-5	143	30.0	56.2	0.431	1.15	
19-6	160	29.3	52.8	0.479	1.21	
19-7	174	28.7	49.7	0.574	1.25	

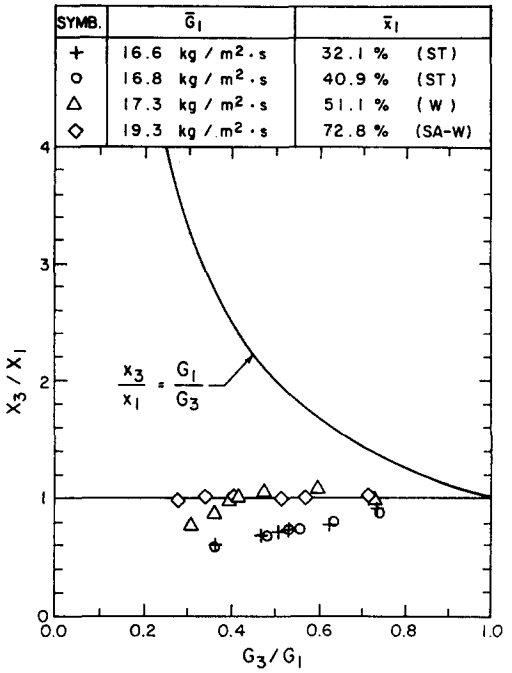

Figure 6. Effect of inlet quality on phase distribution at the lowest mass flux.

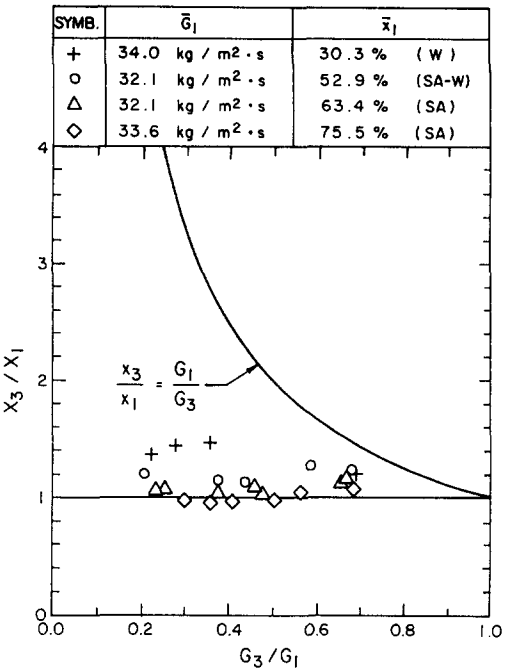

Figure 7. Effect of inlet quality on phase distribution at a high mass flux.

3.1. *Effect of inlet quality*

This effect is illustrated in figures 6 and 7 in which data of the same inlet mass flux but different inlet qualities are presented. Figure 6 shows the trend for the lowest mass flux tested, while figure 7 exemplifies the trend for all other mass fluxes. Values of $\bar{G}_1$ and $\bar{x}_1$ listed in the legend of these and subsequent figures represent the arithmetic average values for each of the 19 test groups (individual values of G_1 and x_1 appear in table 1). The following abbreviations were used for the inlet flow patterns: stratified (ST), wavy (W), semiannular–wavy (SA-W) and semiannular (SA).

From figure 7, which is representative of most of the present data, it is evident that x_3/x_1 decreases with increasing x_1. The change in inlet flow pattern from wavy to semiannular does not seem to interfere with the continuity of this trend. However, figure 6 shows an opposite trend at the lowest G_1 which may be related to the wavy–stratified transition.

3.2. *Effect of inlet mass flux*

This effect is explored in figures 8 and 9 by presenting data at the same inlet quality but different inlet mass fluxes. At a first glance, it appears that G_1 can have a strong influence on the phase distribution represented by the values of x_3/x_1. However, a closer examination reveals that within the data of the same inlet flow pattern, G_1 does not appear to influence x_3/x_1. The influences depicted in figures 8 and 9 appear to be mainly related to inlet flow pattern transitions.

The present trend of insignificant effect of G_1 within the same inlet flow pattern is consistent with Honan & Lahey (1981) for vertical junctions and Saba & Lahey (1984) for horizontal junctions.

3.3. *Effect of inlet superficial liquid velocity*

The data were regrouped in order to show the effect of inlet V_{LS} for fixed values of inlet V_{GS} and a segment of these results is shown in figures 10 and 11. These results, as well as others not shown (Rubel 1986), indicate that W_{L3}/W_{L1} decreases continuously with increasing V_{LS} at a fixed V_{GS}. The interesting feature of this trend is that it is independent of the inlet flow pattern, i.e. the reversal of trend noted in figures 6 and 7 disappears when the same data are replotted as shown in figures 10 and 11. Another interesting feature of this trend is that it shows that the velocity ratio has an important effect on phase distribution (irrespective of flow pattern), which supports the hypothesis used in some of the models discussed later. The investigations of both Hong (1978) and

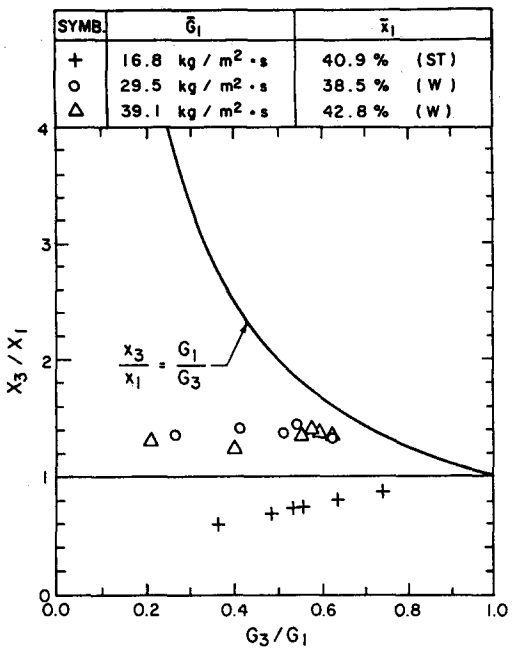

Figure 8. Effect of inlet mass flux on phase distribution at $x_1 \cong 41\%$.

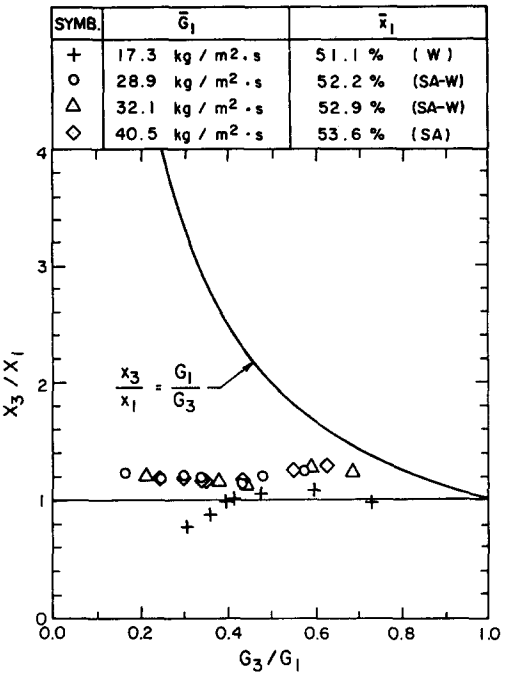

Figure 9. Effect of inlet mass flux on phase distribution at $x_1 \cong 52\%$.

Seeger *et al.* (1986) showed the same effect on phase distribution due to V_{LS}. The inlet flow patterns in these investigations included wavy and annular flow (Hong 1978) and stratified, dispersed bubble, slug and annular flow (Seeger *et al.* 1986).

4. COMPARISON WITH EXISTING CORRELATIONS

4.1. Seeger et al. (1986)

The correlation by Seeger *et al.* (1986) consists of a set of empirically derived equations for different branch orientations, based on their phase-distribution data. The present comparison is carried out keeping in mind that the operating conditions (P_1 and G_1) on which Seeger *et al.* based their correlation are very different from the present conditions. The equation proposed for

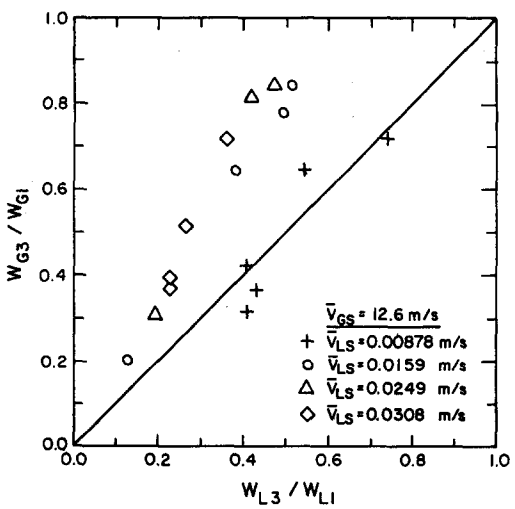

Figure 10. Effect of $\bar{V}_{LS}$ on phase distribution at $\bar{V}_{GS} = 12.6$ m/s.

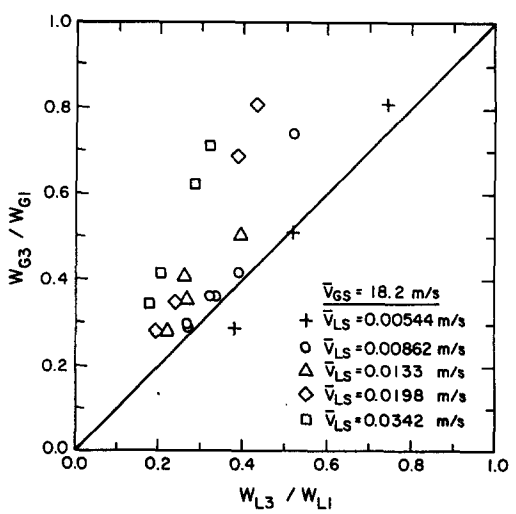

Figure 11. Effect of $\bar{V}_{LS}$ on phase distribution at $\bar{V}_{GS} = 18.2$ m/s.

horizontal main and branch pipes for any inlet flow pattern other than dispersed bubble is

$$\frac{x_3}{x_1} = 5\eta - 6\eta^2 + 2\eta^3 + a\eta(1-\eta)^4, \quad [2]$$

where

$$\eta = \frac{G_3}{G_1}, \quad [3a]$$

$$a = 13.9\left[\left(\frac{\rho_G}{\rho_L} S_1^2\right)^{-0.26} - 1\right], \quad [3b]$$

$$S_1 = \frac{\rho_L}{1-x_1}\left[\frac{1+0.12(1-x_1)}{\rho_{h1}} + \frac{V_{rel}}{G_1} - \frac{x_1}{\rho_G}\right], \quad [3c]$$

$$\rho_{h1} = \left(\frac{x_1}{\rho_G} + \frac{1-x_1}{\rho_L}\right)^{-1} \quad [3d]$$

and

$$V_{rel} = \frac{1.18}{\rho_L^{0.5}}[g\sigma(\rho_L - \rho_G)]^{0.25}; \quad [3e]$$

g and σ are the gravitational acceleration and liquid surface tension, respectively.

Comparison with [2] was made by substituting the experimental values of G_3/G_1, x_1, ρ_G, ρ_L and σ for all data points and computing the corresponding predictions of x_3/x_1. These predictions are compared with the corresponding experimental values in figures 12–14 which are designed to define the particular regions of agreement and disagreement. Figure 12 shows a remarkable agreement with the data corresponding to $G_3/G_1 \geqslant 0.4$ and $x_1 \geqslant 40\%$ with most predictions falling within $\pm$ 20% of the corresponding measured values. This is a very encouraging result considering the differences in operating conditions. For the entire range of x_1 and $G_3/G_1 \geqslant 0.3$, figure 13 shows that most of the data is predicted well (within $\pm$ 40%). Equation [2] is shown in figure 14 to predict poorly the data for low extraction rates ($G_3/G_1 < 0.3$). Seeger *et al.* (1986) also noted a quite large data scatter around [2] with their own data for low G_3/G_1.

4.2. *Azzopardi & Whalley (1982)*

The phase-distribution model proposed by Azzopardi & Whalley (1982) is geometrically based for annular flow. The model assumes that the portion of liquid removed through the branch comes from the same segment of the tube as the removed gas. Furthermore, the model assumes that the liquid which is removed comes from the liquid film; i.e. the liquid which exists as entrained droplets

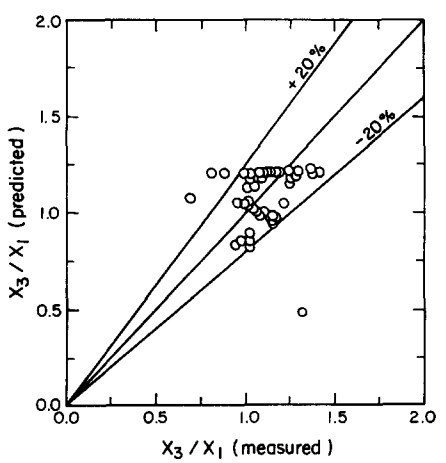

Figure 12. Comparison with correlation by Seeger *et al.* (1986) for $x_1 \geqslant 40\%$ and $G_3/G_1 \geqslant 0.4$.

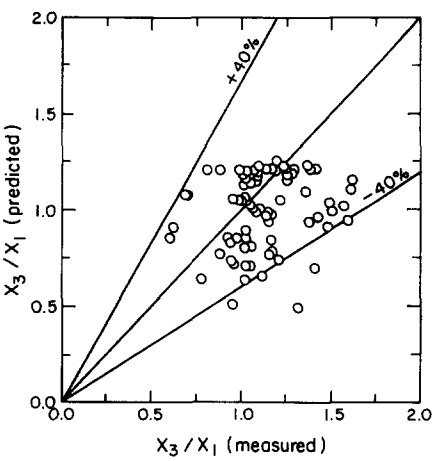

Figure 13. Comparison with correlation by Seeger *et al.* (1986) for all x_1 and $G_3/G_1 \geqslant 0.3$.

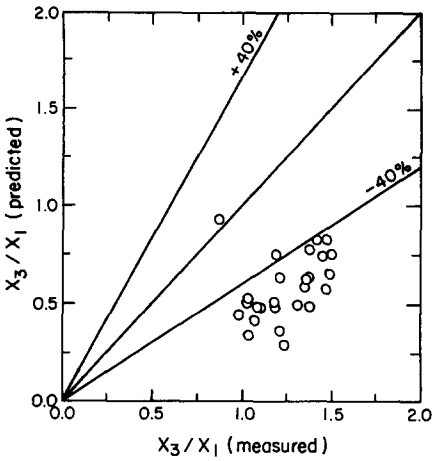

Figure 14. Comparison with correlation by Seeger *et al.* (1986) for all x_1 and $G_3/G_1 < 0.3$.

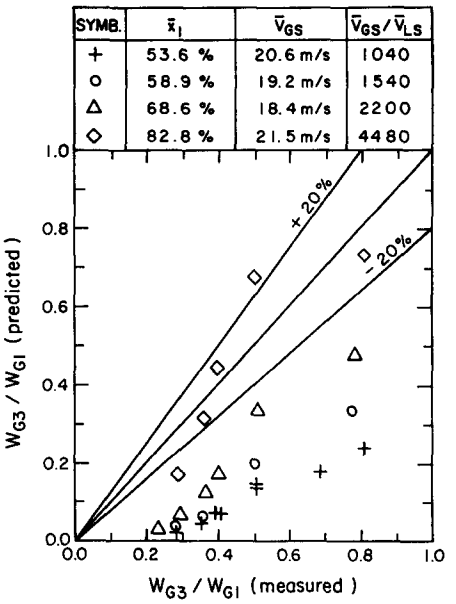

Figure 15. Comparison between data of semiannular flow and the model of Azzopardi & Whalley (1982) for vertical annular flow assuming $E_1 = 0$.

travels straight on into the run. For the special case of vertical upflow where the liquid film thickness is uniform over the entire tube periphery, the model reduces to

$$\frac{W_{G_3}}{W_{G_1}} = \frac{1}{2\pi}\left[\left(\frac{2\pi}{1-E_1}\frac{W_{L3}}{W_{L1}}\right) - \sin\left(\frac{2\pi}{1-E_1}\frac{W_{L3}}{W_{L1}}\right)\right], \quad [4]$$

where E_1 is the fraction of inlet liquid which exists as entrained droplets.

Azzopardi (1984) later proposed a correction term based on data from junctions with different branch-to-inlet diameter ratios (D_3/D_1). Substituting this correction term into [4] gives (for $D_3 = D_1$)

$$\frac{W_{G3}}{W_{G1}} = \frac{1}{2\pi}\left[\left(\frac{1.67\pi}{1-E_1}\frac{W_{L3}}{W_{L1}}\right) - \sin\left(\frac{1.67\pi}{1-E_1}\frac{W_{L3}}{W_{L1}}\right)\right]. \quad [5]$$

The experimental values of W_{G3}/W_{G1} for the data points of semiannular flow were compared with the predictions of [5] at the same W_{L3}/W_{L1}, the result being shown in figure 15. It must be emphasized that good agreement is not expected in view of the fact that the model applies to annular flow with uniform film thickness in a vertical inlet tube while the data correspond to semiannular flow with a thick stratum at the bottom of the horizontal inlet tube. Nevertheless, this comparison is included because it produced an interesting result which seems to support the hypothesis in Azzopardi & Whalley's (1982) model. Figure 15 shows that the data is generally outside the $\pm 20\%$ prediction accuracy with the model predicting lower vapor flow into the branch than experimentally measured. However, the model's predictions become increasingly better as x_1 and V_{GS}/V_{LS} increase, which moves the flow situation closer to the fully-established annular flow. According to the experimental results of Gill & Hewitt (1962) and the model of Katoaka & Ishii (1983), very little entrainment is expected under the present flow conditions; the results in figure 15 are therefore based on $E_1 = 0$ for comparison purposes.

4.3. Hwang et al. (1988)

Hwang *et al.* (1988) developed a new model based on a dividing-streamline concept, and thus it assumes that there is a "zone of influence" for each of the two phases which is bounded by the conduit wall and the appropriate dividing streamline. Incoming vapor and liquid in side 1 of the junction would have to follow curved paths in order to exit through side 3 (the branch) of the junction, as shown in figure 16. The model traces the dividing-streamline paths based on a balance

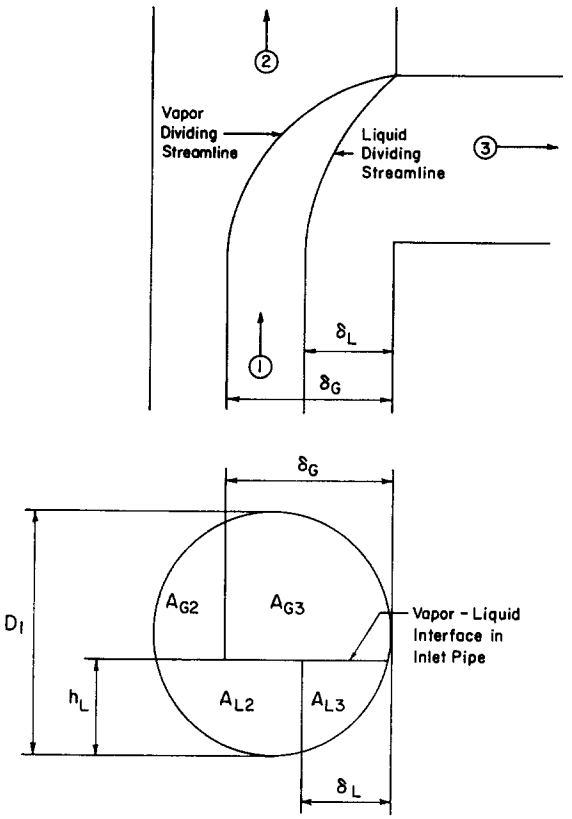

Figure 16. Parameters related to the model by Hwang *et al.* (1988).

between the dominant forces acting on each phase. For separated flow (e.g. wavy or annular), the model simplifies to a balance between centrifugal forces, thus

$$\frac{\rho_G V_G^2}{R_G} = \frac{\rho_L V_L^2}{R_L}, \qquad [6]$$

where R_G and R_L are the radii of curvature of the vapor and liquid dividing streamlines, respectively; and V_G and V_L are the mean velocities of the vapor and liquid phases in side 1 of the junction, respectively, given by

$$V_G = \frac{x_1 G_1}{(\rho_G \alpha_1)} \qquad [7a]$$

and

$$V_L = \frac{(1 - x_1)G_1}{[\rho_L(1 - \alpha_1)]}, \qquad [7b]$$

where α_1 is the inlet void fraction. The radii of curvature R_G and R_L are assumed to follow the relation

$$\frac{R_G}{R_L} = \frac{\left(\frac{\delta_L}{D_1}\right)^{n_L}}{\left(\frac{\delta_G}{D_1}\right)^{n_G}} \qquad [8]$$

where δ_G and δ_L are the depths of the vapor and liquid zones of influence, respectively; shown in figure 16. The exponent n in [8] was determined empirically from a large data base as follows:

$$n_k = 5 + 20 \exp\left[-53\left(\frac{\delta_k}{D_1}\right)\right], \qquad k = G, L. \qquad [9]$$

From [6]–[8] we finally obtain

$$\frac{\left(\frac{\delta_L}{D_1}\right)^{n_L}}{\left(\frac{\delta_G}{D_1}\right)^{n_G}} = \left(\frac{1-\alpha_1}{\alpha_1}\right)^2 \left(\frac{x_1}{1-x_1}\right)^2 \frac{\rho_L}{\rho_G}. \quad [10]$$

A comparison between this model and the present data was made assuming the inlet flow pattern to be wavy for all data points. With this flow geometry and for the cross-section just upstream of the junction (shown in figure 16), the vapor contained in A_{G3} and the liquid contained in A_{L3} flow into the branch (3) while the vapor contained in A_{G2} and the liquid contained in A_{L2} flow into the run (2). Given the values of G_1, x_1, D_1, ρ_L, ρ_G and W_{L3}/W_{L1}, the model was used to calculate the predicted values of W_{G3}/W_{G1} using the following procedure:

1. From the input data, values of α_1 and h_L/D_1, where h_L is the depth of the liquid phase, were calculated using the model of Taitel & Dukler (1976).
2. Assuming uniform velocity within the liquid phase in the inlet [i.e. $W_{L3}/W_{L1} = A_{L3}/(A_{L2} + A_{L3})$ in figure 16] it is possible to calculate δ_L/D_1 from geometrical considerations.
3. The corresponding value of δ_G/D_1 was determined by solving [9] and [10] iteratively.
4. Knowing δ_G/D_1 it is possible to calculate $A_{G3}/(A_{G2} + A_{G3})$ and this ratio is equal to W_{G3}/W_{G1} under the assumption of uniform vapor velocity in the inlet.

Results of this comparison are given in figure 17 which shows the predicted values of x_3/x_1 are within $\pm$ 30% of the corresponding measured values for practically all data points. The scatter is fairly symmetric around the line of perfect prediction. This result significantly supports the physical grounds on which the model of Hwang *et al.* (1988) is based, particularly with the empirical correlation [9] being based on operating conditions quite different from the present ones.

5. CONCLUDING REMARKS

New experimental data on phase distribution have been generated for low-pressure ($111 \leqslant P \leqslant 232$ kPa) steam–water flow in a horizontal T-junction of equal sides (37.6 mm i.d.). The range of inlet flow conditions ($16.1 \leqslant G_1 \leqslant 50.3$ kg/m^2 s and $21.4 \leqslant x_1 \leqslant 86.8\%$) resulted in the

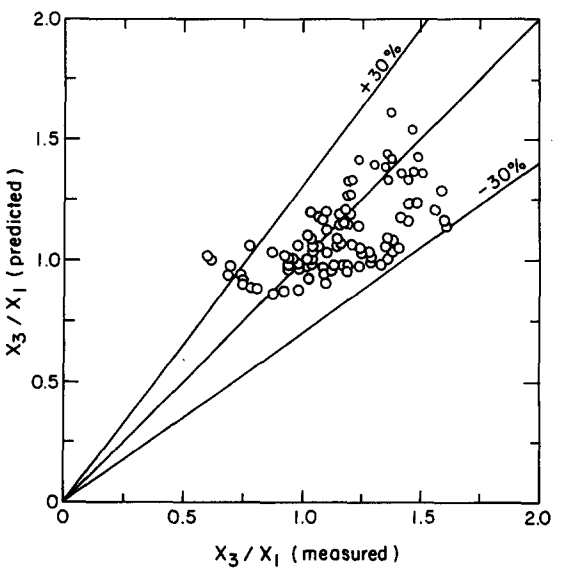

Figure 17. Comparison with the model by Hwang *et al.* (1988).

stratified, wavy, semiannular–wavy and semiannular flow patterns at the junction inlet. Extraction rates within the range 0.15–0.80 were used in generating the phase-distribution data.

The data show that, in general, the phases do not distribute evenly between the two outlets of the junction (i.e. $x_1 \neq x_2 \neq x_3$). For the same G_1, the ratio x_3/x_1 may increase or decrease with increasing x_1 depending on the value of G_1. This reversal of trend may be triggered by a change in the inlet flow pattern (wavy to stratified in the present experiment). Inlet mass flux is shown to be capable of significant effects on x_3/x_1 at fixed values of x_1. However, within the same inlet flow pattern, G_1 does not appear to have any significant effect on phase distribution within the present range of conditions. The data show a consistent trend when V_{GS} was fixed and V_{LS} varied. Irrespective of the inlet flow pattern, it was found that at any given W_{G3}/W_{G1}, W_{L3}/W_{L1} decreases continuously with increasing V_{LS} when V_{GS} was kept constant.

Comparisons with existing correlations developed from, or tuned to, previous data with substantially different P_1, G_1 or x_1 showed surprisingly good agreement. The empirical correlation of Seeger *et al.* (1986) predicted the data well except at low extraction rates. The semiannular flow data approach the predictions of Azzopardi & Whalley (1982) for vertical upward annular flow as x_1 and V_{GS}/V_{LS} increased. A newly proposed model by Hwang *et al.* (1988) predicts x_3/x_1 for the vast majority of data within $\pm 30\%$.

Acknowledgement—Financial support provided by the Natural Sciences and Engineering Research Council of Canada is gratefully acknowledged.

REFERENCES

AZZOPARDI, B. J. 1984 The effect of side arm diameter on the two-phase flow split at a T-junction. *Int. J. Multiphase Flow* **10,** 509–512.

AZZOPARDI, B. J. 1986 Two-phase flow in junctions. In *Encyclopedia of Fluid Mechanics*, Vol. 3, Chap. 25. Gulf, New York.

AZZOPARDI, B. J. & WHALLEY, P. B. 1982 The effect of flow patterns on two-phase flow in a T-junction. *Int. J. Multiphase Flow* **8,** 497–507.

COLLIER, J. G. 1975 Single-phase and two-phase flow behaviour in primary circuit components. Presented at *Symp. on Two-phase Flow and Heat Transfer in Water-cooled Nuclear Reactors*, Dartmouth College, Hanover, N.H.

GILL, L. E. & HEWITT, G. F. 1962 Further data on the upwards annular flow of air–water mixtures. UKAEA Report AERE-R 3935.

HENRY, J. A. R. 1981 Dividing annular flow in a horizontal tee. *Int. J. Multiphase Flow* **7,** 343–355.

HONAN, T. J. & LAHEY, R. T. 1981 The measurement of phase separation in wyes and tees. *Nucl. Engng Des.* **64,** 93–102.

HONG, K. C. 1978 Two-phase flow splitting at a pipe tee. *J. Petrol. Technol.* **30,** 290–296.

HWANG, S. T., SOLIMAN, H. M. & LAHEY, R. T. 1988 Phase separation in dividing two-phase flows. *Int. J. Multiphase Flow* **14,** 439–458.

KATOAKA, I. & ISHII, M. 1983 Entrainment and deposition rates of droplets in annular two-phase flow. *Proc. ASME/JSME therm. Engng Joint Conf.* **1,** 69–80.

LAHEY, R. T. 1986 Current understanding of phase separation mechanisms in branching conduits. *Nucl. Engng Des.* **95,** 145–161.

MANDHANE, J. M., GREGORY, G. A. & AZIZ, K. 1974 A flow pattern map of gas–liquid flow in horizontal pipes. *Int. J. Multiphase Flow* **1,** 537–553.

RUBEL, M. T. 1986 Experimental investigation of phase distribution in a horizontal tee junction. M.Sc. Thesis, Univ. of Manitoba, Winnipeg.

SABA, N. & LAHEY, R. T. 1984 The analysis of phase separation in branching conduits. *Int. J. Multiphase Flow* **10,** 1–20.

SEEGER, W., REIMANN, J. & MULLER, U. 1986 Two-phase flow in a T-junction with a horizontal inlet. Part I: phase separation. *Int. J. Multiphase Flow* **12,** 575–585.

TAITEL, Y. & DUKLER, A. E. 1976 A model for predicting flow regime transitions in horizontal and near horizontal gas–liquid flow. *AIChE Jl* **22,** 47–55.